analytical chemistry

Technical Note

Cite This: Anal. Chem. 2020, 92, 634−639

pubs.acs.org/ac

High-Resolution Reconstruction for Diffusion-Ordered NMR Spectroscopy

Enping Lin, Yu Yang,* Yuqing Huang,* and Zhong Chen

Department of Electronic Science, State Key Laboratory of Physical Chemistry of Solid Surfaces, Xiamen University, Xiamen, Fujian 361005, China

Supporting Information

ABSTRACT: Diffusion-ordered NMR spectroscopy (DOSY) presents an essential tool for the analysis of compound mixtures by revealing intrinsic diffusion behaviors of mixed components. The applicability of DOSY measurements on complex mixtures is generally limited by the performance of data reconstruction algorithms. Here, based on constraints on low rank and sparsity of DOSY data, we propose a reconstruction method to achieve high-resolution DOSY spectra with excellent peak alignments and accurate diffusion coefficients for measurements of complex mixtures even when component signals are congested and mixed together along the spectral dimension. This proposed method is robust and suitable for DOSY data acquired from common commercial NMR instruments; thus, it may broaden the scope of DOSY applications.

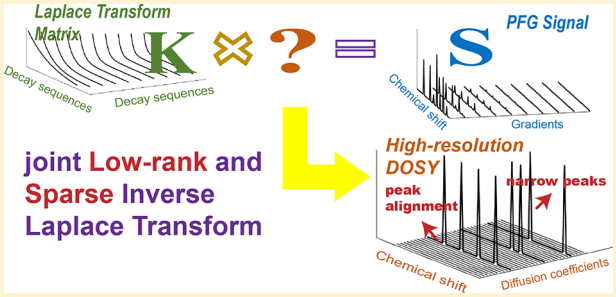

Nuclear magnetic resonance (NMR)[1] constitutes a commonly used technique for compound identification,[2] quantitative detection,[3] and structural analysis[4] in complex mixtures. Diffusion-ordered NMR spectroscopy (DOSY)[5,6] presents an effective tool for identifying chemical substances in mixtures and detecting intermolecular interactions[7] by differentiating NMR signals of a compound mixture according to differences in the molecular translational diffusion. The validation of the resulting DOSY spectra significantly depends on effective data reconstruction algorithms. The most essential functions of DOSY are to resolve overlapping peaks, separate signals from different compounds, and group signals that belong to the identical molecule. Correspondingly, performance of the DOSY reconstruction algorithm is evaluated by the alignment of peaks from the same molecule and the distinguishment of individual peaks (i.e., spectral resolution). A high-resolution DOSY spectrum[8] should have excellent peak alignment and narrow peak width in diffusion dimension. Unfortunately, these two objectives in high-resolution DOSY are difficult to achieve concurrently, particularly for measurements of complex mixtures that contain congested 1D NMR resonances.

DOSY reconstruction methods are roughly divided into two categories, namely exponential fitting and inverse Laplace transform. Exponential fitting, including SPLMOD (spline model),[9,10] CORE (component resolved NMR spectroscopy),[11] DECRA (direct exponential curve resolution algorithm),[12,13] SCORE (speedy component resolved NMR spectroscopy),[14] and MRC (multivariate curve resolution),[15,16] among others,[17] requires the accurate number of molecular components in advance, which generally leads to unstable and invalid reconstruction spectra if inaccurate number estimation of molecular components is provided. Different from exponential fitting, the inverse Laplace transform dispenses with the number of molecular components as a prerequisite. These methods are implemented based on the fact that decay signals along the gradient dimension and diffusion distribution signals along the diffusion dimension constitute a Laplace transform pair[18] (i.e., diffusion distribution signals are the Laplace transform of the gradient field decay signals). Many optimization methods for solving the inverse problem have been proposed for DOSY reconstruction, such as the nonnegative least-squares (NNLS) method,[19] Tikhonov regularization method,[20] constrained regularization (CONTIN),[20,21] entropy maximization (MaxEnt),[22] iterative thresholding algorithm for multiexponential decay (ITAMed),[23] sparse and Tikhonov combined regularization method,[24] and others.[25,26] These methods are basically designed for 1D reconstruction. Therefore, to obtain the 2D DOSY spectrum, each row of the spectrum corresponding to each frequency component is reconstructed individually, which would induce misalignment of peaks in the diffusion dimension due to inevitable computational errors. To address this issue, Yuan et al. proposed a 2D method called simultaneous inversion of Laplace transform (SILT),[27] which exploits the low-rank property of 2D DOSY spectrum data and uses nuclear norm for regularization constraint. The 2D low-rank property works like a spectral comb to increase peak alignment along the diffusion dimension but with an undesirable effect of peak

Received: August 23, 2019
Accepted: November 26, 2019
Published: November 26, 2019

DOI: 10.1021/acs.analchem.9b03865
Anal. Chem. 2020, 92, 634−639

broadening and might even induce some artifacts under the worst-case scenario, which does not satisfy the criteria of high-resolution DOSY. From Figure 1(a) and (b), it can be seen

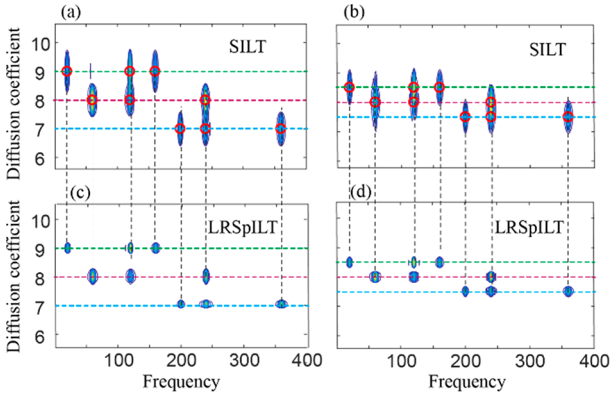

Figure 1. Reconstructed spectra of SILT and LRSpILT on two simulated data sets. SILT results of mixture 1 (a) and mixture 2 (b). LRSpILT results of mixture 1 (c) and mixture 2 (d). Red circles denote ideal peak positions. Simulated data parameters are detailed in the Supporting Information.

that peak broadening in reconstructed spectra by SILT increases the difficulty in distinguishing molecular components with close diffusion coefficients.

In this work, we propose a general 2D inverse Laplace transform method, called low-rank and sparse inverse Laplace transform (LRSpILT), for high-resolution DOSY reconstruction on complex mixtures. This method is designed based on the joint constraints on low-rank and sparsity of DOSY data[28,29] to achieve excellent peak alignment and accurate diffusion coefficient estimation with narrow peak width in the diffusion dimension, thus leading to high-resolution DOSY reconstruction. As Figure 1 (c) and (d) show, LRSpILT maintains the alignment of peaks with the same diffusion coefficients and gives results with narrowed peaks in the diffusion dimension, which represents reduced estimation uncertainty of diffusion coefficients. The resulting spectra present significantly improved resolution and satisfactory distinguishment between adjacent peaks compared to SILT.

METHODS

A pulse field gradient (PFG) signal is a kind of decay signal similar to relaxation signals that decay with evolution time. To obtain the decay rates of these signals, one should apply inverse Laplace transform (ILT) or exponential fitting instead of Fourier transform, which is suitable for analysis of frequency but not decay rate (detailed in Supporting Information).

Exponential fitting methods aim to obtain decay rates by minimizing the error between acquired signal and exponential fitting model, which can be modeled as

$$\min_{x_i,\alpha_i} \left|\left| \sum_{i=1}^{N} x_i \mathbf{e}^{-\alpha_i \mathbf{t}} - \mathbf{s}(\mathbf{t}) \right|\right|_2 \tag{1}$$

where $\mathbf{t} \in \mathbb{R}^p$ is the evolution time vector with p time points, $\mathbf{s}(\mathbf{t}) \in \mathbb{R}^p$ is the acquired decay signal vector, x_i and α_i are estimated intensity and decay rate of the i-th exponential decay component, respectively, and N is the number of exponential decay components, which is 1 for monoexponential fitting and 2 for double exponential fitting. For signals decaying with gradient strength, e.g. the DOSY signal, the objective function is modified as

$$\min_{x_i,\alpha_i} \left|\left| \sum_{i=1}^{N} x_i \mathbf{e}^{-\alpha_i \mathbf{g}^2} - \mathbf{s}(\mathbf{g}^2) \right|\right|_2^2 \tag{2}$$

where $\mathbf{g}$ is the gradient vector. Without loss of generality, we apply the model of the gradient field decay signal for the rest of the paper. Eq 2 requires a given N to perform the fitting, and different N would lead to different results.

To relax the assumption of the exponential fitting method, ILT implements a different strategy, where the specific values of α_i are not required to be estimated but given as grid points on the range of interest, and N is the number of grid points. Then, eq 2 can be reformulated into the matrix form:

$$\min_{\mathbf{x}} \|\mathbf{K}\mathbf{x} - \mathbf{s}\|_2^2 \tag{3}$$

where $\mathbf{K} \in \mathbb{R}^{p\times N}$, each column of $\mathbf{K}$ represents one exponential decay component, and $\mathbf{x} = [x_1, x_2, ..., x_N]^T$ represents the intensities or contributions of each component. We can infer by eq 3 that ILT decomposes PFG signal $\mathbf{s}$ into a group of exponential decay signals, like Fourier transform decomposes signals into a group of frequency signals. But, different from the linear and unitary Fourier transform, the ILT problem is ill-posed, which means there are infinite number of possible solutions for eq 3. For this reason, more constraints should be given to the estimated solution to ensure a reasonable result.

LRSpILT penalizes the rank and data intensities of the reconstructed spectra to control the level of complexity of the result. Thus, the result for LRSpILT should possess the property of joint Low-Rank and sparsity, which suggests that our desired result should be composed of less exponential decay components and these components should be well-aligned. The optimization model[29] of LRSpILT is

$$\mathbf{X} = \arg\min_{\mathbf{X}\geq\mathbf{0}} \frac{1}{2}\|\mathbf{K}\mathbf{X} - \mathbf{S}\|_F^2 + \lambda_1 \|\mathbf{X}\|_{*,b} + \lambda_2 \|\mathbf{X}\|_{1,\mathbf{A}} \tag{4}$$

where $\mathbf{S} \in \mathbb{R}^{p\times m}$ is the 2D discretized gradient field decay signal, which can be easily obtained from the FID data with 1D Fourier transform. $\mathbf{X} \in \mathbb{R}^{N\times m}$ is the estimated DOSY spectra data matrix. $\mathbf{X} \geq \mathbf{0}$ constrains non-negativity of all elements in $\mathbf{X}$. $\|\bullet\|_{*,b}$ is the weighted nuclear norm with the weighted factor vector $\boldsymbol{b} \in \mathbb{R}^r$, which constrains the low-rank of $\mathbf{X}$. The weighted nuclear norm is defined as

$$\|\mathbf{X}\|_{*,\mathbf{b}} = \sum_{i=1}^{r} b_i \sigma_i$$

where σ_i is the i-th singular value of $\mathbf{X}$, and r is the rank of $\mathbf{X}$. $\|\bullet\|_{1,\mathbf{A}}$ is the weighted l_1 norm of the matrix, and $\mathbf{A}$ is the weighted factor matrix which constrains the sparsity of $\mathbf{X}$. λ_1 and λ_2 denote the regularized parameters, which trade off fidelity, low-rank, and sparsity of $\mathbf{X}$. A more detailed discussion on the proposed model and its relation to other methods is given in the Supporting Information.

Proper setting of λ_1 and λ_2 is vital for high-resolution reconstruction. Generally, good choices of λ_1 and λ_2 would be in the range of $\sim 10^{-4}$ to 10^{-1}. Both values of λ_1 and λ_2 might need to be modified according to the specific case. When trying to adjust these two parameters, one can begin with λ_2 =

DOI: 10.1021/acs.analchem.9b03865
Anal. Chem. 2020, 92, 634−639

0 or a small number, and adjust λ_1 to obtain a spectrum with good peak alignment. Then, one can enlarge λ_2 until the spectral resolution is acceptable, which means all the diffusion groups are well-resolved. It is important that λ_2 should not be too large, otherwise essential peaks might disappear or shrink in the spectra. More detailed discussions and demonstrations on the effects of λ_1 and λ_2 are given in the Supporting Information.

We exploit the Alternative Direction Multiplier Method (ADMM)[29] to solve eq 4, and the corresponding mathematical derivation is given in the Supporting Information. Our algorithm is programed in Matlab R2016b, and the source codes are available upon the request by emailing the authors and can also be downloaded from ref 30 for free.

Although LRSpILT is devised specifically for high-resolution DOSY reconstruction, it might also fit for other analyses of exponential decay signals such as Altered Relaxation Times Allow Detection of Exchange Correlation (NMR ARTDECO) spectra,[31] low field NMR T_2 distribution, and high field ^{1}H NMR T_2 relaxation signals.

EXPERIMENTAL SECTION

To evaluate the performance in a practical situation, we tested the proposed method on two experimental data sets. The first experimental data set is named QGC,[32] consisting of quinine (100 mM/L), geraniol (100 mM/L), and camphene (200 mM/L) dissolved in deuterated methanol. The pulsed field gradient experiments were performed at 297 K on a Varian 500 MHz spectrometer equipped with a 5 mm XYZ indirect detection probe. The "BPPSTE" DOSY pulse sequence was used with the diffusion delay 0.04 s and a net diffusion-encoding pulse width of 2 ms. Twenty-five diffusion gradients GD were applied with the incremental amplitudes from 1.46 to 40.62 G/cm. A spectral width of 12 ppm was used, and 16 384 complex data points were acquired with 64 scans for each gradient strength, acquisition time of 1.99 s, and relaxation delay of 2.0 s. A total of 65 536 complex data points were Fourier transformed using a Gaussian window with a line broadening value of 1.0 Hz. Only the spectral region 2−14 ppm was displayed.

The second experimental data set named M6[27] consisting of methanol (2 μL), ethanol (4 μL), 1-butanol (8 μL), threonine (11.12 mg), lysine (12.58 mg), and sucrose (21.16 mg) dissolved in D_2O (450 μl) was prepared. The pulsed field gradient experiments were performed at 298 K on another Bruker AVANCE 600 spectrometer equipped with a CryoProbe (1 H frequency 600.13 MHz). The Bruker pulse sequence "ledbpgppr2s" was used with diffusion delay 0.16 s and a net diffusion-encoding pulse width (d) of 2 ms. Water signal was suppressed with presaturation. 32 gradient strengths ranging from 1.465 to 46.4 G/cm were chosen to give linear space in nominal gradient. A spectral width of 20 ppm was used, and 16 384 complex data points were acquired with 8 scans for each gradient strength, acquisition time of 1.363 s, and relaxation delay of 2.5 s. A total of 65 536 complex data points were Fourier transformed using an exponential window with a line broadening value of 0.5 Hz. Only the spectral region 0.5−5.5 ppm was displayed.

RESULTS AND DISCUSSION

Figure 2 shows results of monoexponential fitting,[25] SILT,[27] and LRSpILT on experimental data of mixture QGC.[32] From

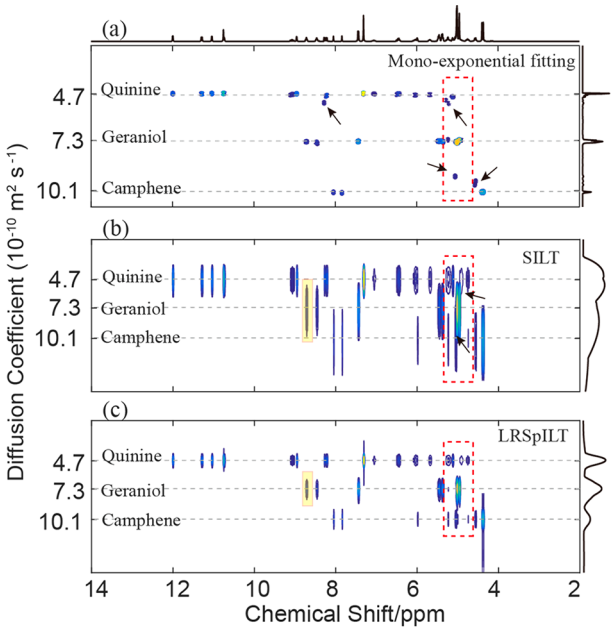

Figure 2. Reconstructed spectra for experimental data QGC with (a) monoexponential fitting, (b) SILT, and (c) LRSpILT. Areas marked by the red rectangular are of overlapping peaks. Artifacts in (b) and (c) are marked with black arrows. Highlighted areas are projected onto the diffusion coefficient dimension and shown in Figure S4 of the Supporting Information. The center diffusion coefficient values of components are marked with gray dashed lines.

Figure 2(a), it can be seen that spectral peaks of monoexponential fitting reconstructed spectra have some deviation from the reference lines and even artifacts, which might give rise to incorrect analysis of molecular components. From the comparison, it is clear that peaks are broadened along the diffusion dimension, and serious peak overlapping is observed in the SILT reconstructed spectra (Figure 2b), while peak broadening is effectively suppressed. All peaks are well-distinguished along the diffusion dimension in the LRSpILT spectra. It is worth noting that peak alignments are maintained well in both SILT and LRSpILT spectra. From 1D projection spectra on the diffusion dimension, we can intuitively observe that monoexponential fitting leads to small diffusion artifacts (Figure 2 (a)) which are due to the peak misalignment in the diffusion dimension, and SILT cannot perform well for the separation of three molecular components due to the peak broadening (Figure 2 (b)). The LRSpILT result can show exactly three well-separated peak groups corresponding to the three molecular components.

For further quantitative analysis, we define reconstructed spectra resolution (RcSR) to measure the resolution of reconstructed spectral peaks in the diffusion coefficient dimension, formulated as eq 5:

$$\mathrm{RcSR} = \frac{1}{\mathrm{WHH}} \tag{5}$$

where WHH denotes width at half height of the peak. It should be mentioned that we do not compare the RcSR of monoexponential fitting results with that of LRSpILT, as these two methods have totally different mechanisms. The monoexponential fitting method involves univariate processing, and it processes each decay signal individually and generates a pseudo-2D spectrum, where each peak is generated in

DOI: 10.1021/acs.analchem.9b03865
Anal. Chem. 2020, 92, 634−639

Gaussian line shape with the line width determined by the statistics of the fitting.[25] In contrast, for the inverse Laplace transform-based methods, SILT and our proposed LRSpILT involve multivariate processing and generate the whole spectra simultaneously with no constraint on the line shape of each peak. Therefore, only spectral resolutions and spectra of separated 1D components (Figure 3 and Figure 5) of the SILT and LRSpILT are compared.

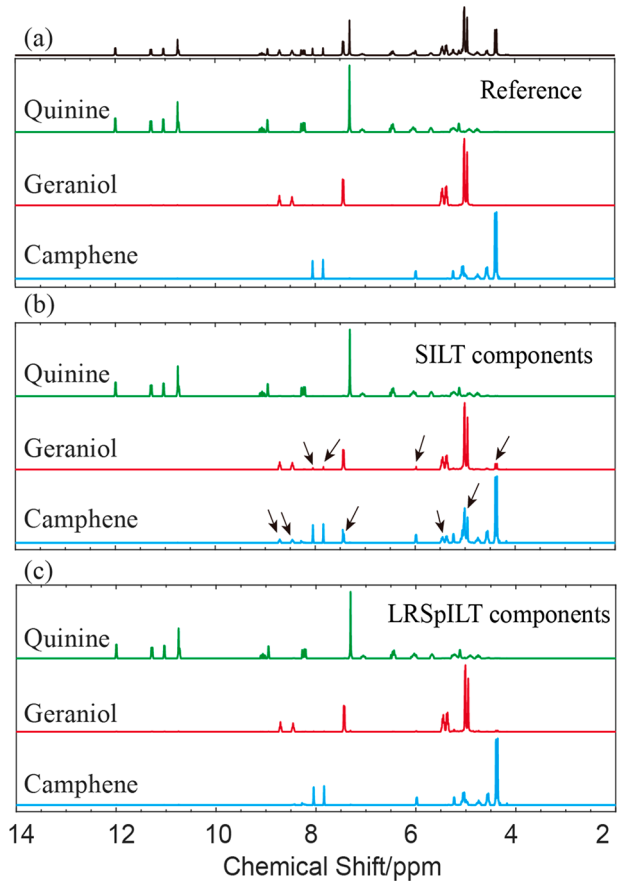

Figure 3. ^{1}H spectra of mixture QGC. (a) Reference spectra of three components: quinine, geraniol, and camphene. (b) Resolved spectra of the three components by SILT. (c) Resolved spectra of the three components by LRSpILT. In (b), artifacts are marked with black arrows. Panels (b) and (c) are both extracted by summarizing a small range across the center diffusion coefficient value (marked with gray dashed lines in Figure 2) for comparison.

The WHHs of corresponding spectral peaks in SILT and LRSpILT reconstructed spectra as highlighted in Figure 2 (b) and (c) are 4 and 1.1 (10^{-10} m^2s^{-1}), respectively (detailed projected peak analysis is shown in Figure S4 in the Supporting Information). Therefore, for this case, the RcSR of LRSpILT reconstructed spectra is approximately 3.64 times greater than that of SILT reconstructed spectra. It indicates that LRSpILT reduces the peak line width (or uncertainty) attributed to the penalty of l_1 norm in eq 4 to encourage a sparse result, which means a narrowed peak and simplified spectra. Further analysis of molecular components can be performed by extracting spectra of each molecular component.

From spectra of separated 1D components shown in Figure 3, we can see that there are clearly some artifacts in SILT results (Figure 3 (b)), while LRSpILT results present more accurate diffusion measurements with higher resolution in the diffusion dimension (Figure 3 (c)).

It is noteworthy that for 1D component separation of SILT reconstructed spectra, because of low spectral resolution, the non-negative matrix factorization (NMF) method[33] is usually applied which would introduce extra computational error and instability due to the nonconvexity of NMF, while NMF is unnecessary for LRSpILT results analysis because the 1D spectra can be directly extracted by summarizing a small range across the center diffusion coefficient values (marked with gray dashed lines in Figures 2 and 4) attributed to high spectral resolution and well-separated molecular components.

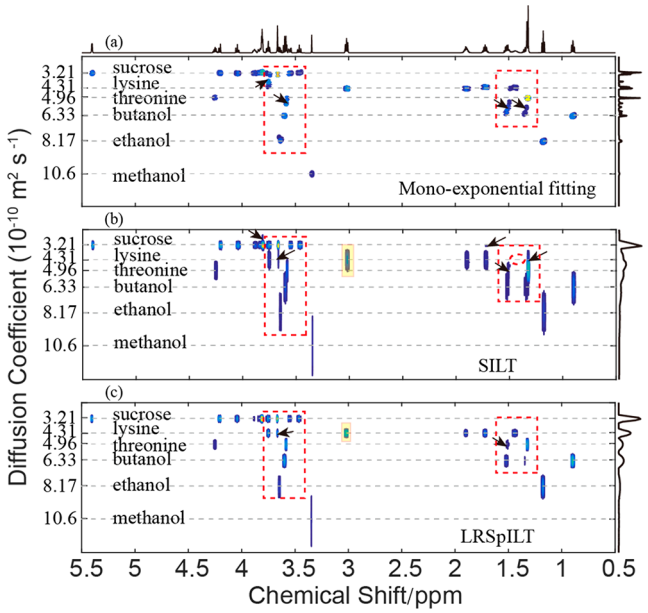

Figure 4. Reconstructed spectra for experimental data M6 with (a) monoexponential fitting, (b) SILT, and (c) LRSpILT. A missing peak in (b) is marked with a red circle. Artifacts in (b) and (c) are marked with black arrows. Areas surrounded by a red rectangular are overlapped peaks. The center diffusion coefficient values of components are marked with gray dashed lines.

Figure 4 shows DOSY reconstruction spectra of M6 with monoexponential fitting,[25] SILT,[27] and LRSpILT. The monoexponential fitting result shows artifacts and scattered spectral peaks (Figure 4 (a)), which lead to errors of spectral components classification and affect further analysis. SILT reconstructed spectral peaks are well-aligned, but peak broadening is observed in the diffusion dimension, resulting in overlap of adjacent peaks (Figure 4 (b)). Compared to the SILT result, the LRSpILT result (Figure 4 (c)), presenting high-resolution DOSY manner with narrow spectral peaks and excellent peak alignments, can reduce artifacts and provide more accurate diffusion interpretation of the data.

From the 1D projection spectra along the diffusion dimension, it is clear that monoexponential fitting result (Figure 4 (a)) has many artifacts, which might lead to an overestimation of the number of components in the mixture, and SILT result (Figure 4 (b)) cannot clearly distinguish the six components due to the spectral broadening. As a comparison, these six components are clearly distinguished from the 1D projection spectrum of LRSpILT reconstructed spectra (Figure 4 (c)), except that the methanol peak is weak because of its relatively small amount in the mixture. The RcSR

DOI: 10.1021/acs.analchem.9b03865
Anal. Chem. 2020, 92, 634−639

analysis (detailed in Supporting Information) implies that the resolution of LRSpILT reconstructed spectra is approximately 2.23 times higher than that of SILT.

Component separation analysis (Figure 5) shows that LRSpILT significantly reduces artifacts compared to the SILT. However, we also note that the spectral peaks of LRSpILT shrink in several positions. Two main reasons of this peak shrinkage are as follows. First, sparse regularization constraint tends to obtain narrower peaks which better satisfy sparse assumption. Second, to improve the reconstruction efficiency, a threshold operation is performed before the reconstruction, i.e. the spectral points below threshold are set to zero, which would cause the shrinkage of peaks. However, the narrowing of some peak normally does not affect the following distinguishment of mixture components. In some cases, if the shrinkage of peaks is unacceptable, one could decrease the sparsity regularization parameter λ_2 in eq 3 or lower the threshold value before the reconstruction.

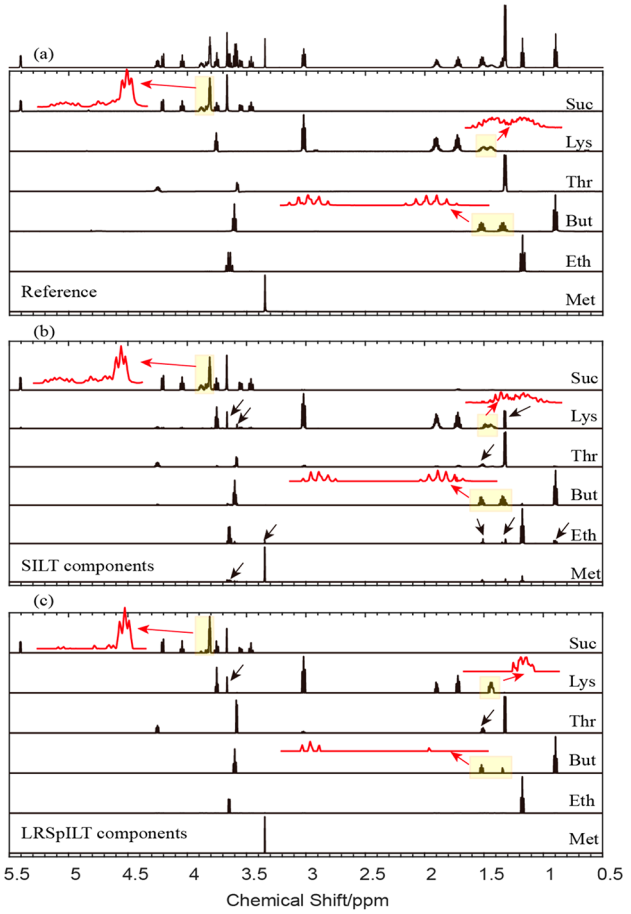

Figure 5. ^{1}H spectra of mixture M6. (a) Reference spectra of six components: sucrose (Suc), lysine (Lys), threonine (Thr), butanol (But), ethanol (Eth), and methanol (Met). (b) Resolved spectra of the six components by SILT. (c) Resolved spectra of the six components by LRSpILT. In (b) and (c), artifacts are marked with black arrows. Highlighted areas, where spectral line shape is not recovered well by LRSpILT, are zoomed in and shown in red. Panels (b) and (c) are both extracted by summarizing a small range across the center diffusion coefficient values (marked with gray dashed lines in Figure 4) for comparison.

CONCLUSIONS

In conclusion, we propose a DOSY reconstruction approach, LRSpILT, to obtain 2D high-resolution DOSY spectra with excellent peak alignment and narrow spectral peaks for measurements of complex mixtures. Simulated and experimental results suggest that the proposed method enjoys an advantage of high spectral resolution along the diffusion dimension. Further extraction of component molecular signals from reconstructed spectra demonstrates that the proposed method is robust and accurate for the analysis of the compound mixture, even when its component signals are congested and mixed together along the spectral dimension. Further, this method can be robustly applied to DOSY data acquired from standard commercial NMR instruments for high-resolution DOSY reconstruction. Therefore, it might broaden the scope of DOSY applications for identification and analysis of complex mixtures that contain congested or even overlapped NMR resonances.

ASSOCIATED CONTENT

Supporting Information

The Supporting Information is available free of charge at https://pubs.acs.org/doi/10.1021/acs.analchem.9b03865.

Section A: methodology of the spectrum reconstruction based on inverse Laplace transform and its relation with Fourier transform and exponential fitting; Section B: effect of regularization parameters on the results; Section C: preprocessing and other technical details; Section D: derivation of the optimization algorithm for LRSpILT; Section E: simulated data parameters in Figure 1; Section F: spectral resolution analysis (PDF)

AUTHOR INFORMATION

Corresponding Authors

*E-mail: yuyang15@xmu.edu.cn.
*E-mail: yqhuangw@xmu.edu.cn.

ORCID

Yuqing Huang: 0000-0003-0606-1165
Zhong Chen: 0000-0002-1473-2224

Notes

The authors declare no competing financial interest.

ACKNOWLEDGMENTS

This work was partially supported by the National Natural Science Foundation of China (Grants 61601386 and 11675135), the Key Science and Technique Project of Fujian Province of China (Grant 2017H0040), and the Fundamental Research Funds for the Central University (Grant 20720180067). We thank Dr. B. Yuan (one of the authors of ref 28) for sharing the experimental data of M6 and source codes.

REFERENCES

(1) Wang, S.; Parthasarathy, S.; Xiao, Y.; Nishiyama, Y.; Long, F.; Matsuda, I.; Endo, Y.; Nemoto, T.; Yamauchi, K.; Asakura, T. *Chem. Commun.* **2015**, *51*, 15055−15058.
(2) Wei, X.; Koo, I.; Kim, S.; Zhang, X. *Analyst* **2014**, *139*, 2507−2514.
(3) Takeuchi, M.; Kawashima, H.; Imai, H.; Fu-jii, S.; Oaki, Y. *J. Mater. Chem. C* **2019**, *7*, 4089−4095.
(4) Hameury, S.; Frémont, P. D.; Braunstein, P. *Chem. Soc. Rev.* **2017**, *46*, 632−733.

DOI: 10.1021/acs.analchem.9b03865
Anal. Chem. 2020, 92, 634−639

(5) Groves, P. *Polym. Chem.* **2017**, *8*, 6700−6708.
(6) Pagès, G.; Gilard, V.; Martino, R.; Malet-Martino, M. *Analyst* **2017**, *142*, 3771−3796.
(7) Yu, M.; Meng, L.; Li, H.; Zhang, C. *CrystEngComm* **2017**, *19*, 3145−3155.
(8) Cabrita, E. J.; Berger, S.; Brauer, P.; Karger, J. *J. Magn. Reson.* **2002**, *157*, 124−131.
(9) Provencher, S. W.; Vogel, R. H. In *Numerical Treatment of Inverse Problems in Differential and Integral Equations*, 1st ed.; Deuflhard, P., Hairer, E., Eds.; Birkhäuser: Boston, Secaucus, United States, 1983; Vol. 2, pp 304−319.
(10) Vogel, R. H. *SPLMOD Users Manual (Ver. 3)*; Data Analysis Group, EMBL: Heidelberg, 1988.
(11) Stilbs, P.; Paulsen, K.; Griffiths, P. C. *J. Phys. Chem.* **1996**, *100*, 8180−8189.
(12) Windig, W.; Antalek, B. *Chemom. Intell. Lab. Syst.* **1997**, *37*, 241−254.
(13) Antalek, B.; Windig, W. *J. Am. Chem. Soc.* **1996**, *118*, 10331−10332.
(14) Nilsson, M.; Morris, G. A. *Anal. Chem.* **2008**, *80*, 3777−3782.
(15) Huo, R.; Wehrens, R.; Buydens, L. M. C. *J. Magn. Reson.* **2004**, *169*, 257−269.
(16) Gorkom, L. C. M. V.; Hancewicz, T. M. *J. Magn. Reson.* **1998**, *130*, 125−130.
(17) Provencher, S. W. *J. Chem. Phys.* **1976**, *64*, 2772−2777.
(18) Archer, B. R.; Wagner, L. K. *Med. Phys.* **1982**, *9*, 844.
(19) Charles, L. L.; Richard, J. H. In *Solving Least Squares Problems*; Society for Industrial and Applied Mathematics: Philadelphia, 1995.
(20) Day, I. J. *J. Magn. Reson.* **2011**, *211*, 178−185.
(21) Morris, K. F.; Johnson, C. S. *J. Am. Chem. Soc.* **1993**, *115*, 4291−4299.
(22) Provencher, S. W. *Comput. Phys. Commun.* **1982**, *27*, 213−227.
(23) Delsuc, M.-A.; Malliavin, T. E. *Anal. Chem.* **1998**, *70*, 2146−2148.
(24) Berman, P.; Levi, O.; Parmet, Y.; Saunders, M.; Wiesman, Z. *Concepts Magn. Reson., Part A* **2013**, *42*, 72−88.
(25) Nilsson, M. *J. Magn. Reson.* **2009**, *200*, 296−302.
(26) Xu, K.; Zhang, S. *Anal. Chem.* **2014**, *86*, 592−599.
(27) Yuan, B.; Ding, Y.; Kamal, G. M.; Shao, L.; Zhou, Z.; Jiang, B.; Sun, P.; Zhang, X.; Liu, M. *J. Magn. Reson.* **2017**, *278*, 1−7.
(28) Zhuang, L.; Gao, S.; Tang, J.; Wang, J.; Lin, Z.; Ma, Y.; Yu, N. *IEEE Trans. Image Process.* **2015**, *24*, 3717−3728.
(29) Giampouras, P.; Themelis, K.; Rontogiannis, A.; Koutroumbas, K. *IEEE Trans.Geosci. Remote.* **2016**, *54*, 4775−4789.
(30) Lin, E. Codes for High-Resolution Reconstruction for Diffusion-Ordered NMR Spectroscopy. https://github.com/EricLin1993/Eric_GitHub.
(31) Lee, J. H.; Labadie, C.; Springer, C.; Harbison, G. *J. Am. Chem. Soc.* **1993**, *115*, 7761−7764.
(32) Foroozandeh, M.; Castañar, L.; Martins, L. G.; Sinnaeve, D.; Poggetto, G. D.; Tormena, C. F.; Adams, R. W.; Morris, G. A.; Nilsson, M. *Angew. Chem.* **2016**, *128*, 15808−15811.
(33) Kim, J.; Park, H. In *Eighth IEEE International Conference on Data Mining*; Washington, DC, 2008; pp 353−362.

DOI: 10.1021/acs.analchem.9b03865
Anal. Chem. 2020, 92, 634−639